Chinese Journal of Natural Medicines

Gypensapogenin I ameliorates liver fibrosis by targeting MST1, restoring Hippo pathway homeostasis, and inhibiting HSCs activation

Kexin Huang, Xiaoxu Chen, Hanbo Pei, Nan Yang, Yuxin Miao, Xiaoshu Zhang, Jiayin Yue

Citation: Kexin Huang, Xiaoxu Chen, Hanbo Pei, Nan Yang, Yuxin Miao, Xiaoshu Zhang, Jiayin Yue, Gypensapogenin I ameliorates liver fibrosis by targeting MST1, restoring Hippo pathway homeostasis, and inhibiting HSCs activation, Chinese Journal of Natural Medicines, 2026, 24(10), 1237−1250. doi: 10.1016/S1875−5364(26)61217−4.

View online: https://doi.org/10.1016/S1875−5364(26)61217−4

Related articles that may interest you

Picroside II promotes HSC apoptosis and inhibits the cholestatic liver fibrosis in Mdr2$^{-/-}$ mice by polarizing M1 macrophages and balancing immune responses

Chinese Journal of Natural Medicines. 2024, 22(7), 582−598 https://doi.org/10.1016/S1875−5364(24)60571−6

Ligustroflavone ameliorates CCl_4−induced liver fibrosis through down−regulating the TGF−β/Smad signaling pathway

Chinese Journal of Natural Medicines. 2021, 19(3), 170−180 https://doi.org/10.1016/S1875−5364(21)60018−3

Si−Wu−Tang attenuates liver fibrosis *via* regulating lncRNA H19−dependent pathways involving cytoskeleton remodeling and ECM deposition

Chinese Journal of Natural Medicines. 2024, 22(1), 31−46 https://doi.org/10.1016/S1875−5364(24)60560−1

Mechanisms exploration of Angelicae Sinensis Radix and Ligusticum Chuanxiong Rhizoma herb−pair for liver fibrosis prevention based on network pharmacology and experimental pharmacologylogy

Chinese Journal of Natural Medicines. 2021, 19(4), 241−254 https://doi.org/10.1016/S1875−5364(21)60026−2

Chuanxiong Rhizoma extracts prevent cholestatic liver injury by targeting H3K9ac−mediated and cholangiocyte−derived secretory protein PAI−1 and FN

Chinese Journal of Natural Medicines. 2023, 21(9), 694−709 https://doi.org/10.1016/S1875−5364(23)60416−9

Dammarane−type triterpenoid saponins isolated from *Gynostemma pentaphyllum* ameliorate liver fibrosis *via* agonizing PP2C α and inhibiting deposition of extracellular matrix

Chinese Journal of Natural Medicines. 2023, 21(8), 599−609 https://doi.org/10.1016/S1875−5364(23)60395−4

Wechat

Chinese Journal of Natural Medicines 24 (2026) 1237-1250

Contents lists available at ScienceDirect

Chinese Journal of Natural Medicines

journal homepage: www.cjnmcpu.com/



Original article

Gypensapogenin I ameliorates liver fibrosis by targeting MST1, restoring Hippo pathway homeostasis, and inhibiting HSCs activation

Kexin Huang[a,Δ], Xiaoxu Chen[b,Δ], Hanbo Pei[a,Δ], Nan Yang[a], Yuxin Miao[a], Xiaoshu Zhang[a, b,*], Jiayin Yue[c,*]

[a] *School of Functional Food and Wine, Shenyang Pharmaceutical University, Shenyang 110016, China*
[b] *School of Traditional Chinese Materia Medica, Shenyang Pharmaceutical University, Shenyang 110016, China*
[c] *School of Pharmacy, Shenyang Medical College, Shenyang 110034, China*

ARTICLE INFO

Article history:
Received 23 May 2026
Revised 24 July 2026
Accepted 26 July 2026
Available online 20 October 2026

Keywords:
Gypensapogenin I
Liver fibrosis
HSCs activation
MST1
Hippo pathway

ABSTRACT

Gypensapogenin I (GI) is a new dammarane type triterpenoid saponin extracted from *Gynostemma pentaphyllum*. This study explored the therapeutic potential and mechanism of GI on liver fibrosis (LF). LF is a key pathological stage of chronic liver disease, and the current treatment is limited. In the mouse LF model induced by carbon tetrachloride (CCl_4) and the LX-2 hepatic stellate cell model activated by transforming growth factor-β1 (TGF-β1), GI showed significant antifibrotic effects *in vitro* and *in vivo*, and could reduce liver injury, inflammation, collagen deposition and cell activation. Mechanistic studies have shown that GI exerts its effect by directly targeting MST1 protein. The direct and specific interaction between GI and MST1 was confirmed by surface plasmon resonance (SPR), drug affinity reaction target stability (DARTS) and cell thermal transition analysis (CETSA). Site directed mutagenesis further identified Arg181 as a key residue necessary for the stable binding of GI to MST1. This binding activated the Hippo signaling pathway, promoted the phosphorylation of MST1, LATS1/2 and YAP, resulting in the retention and inactivation of YAP in the cytoplasm. More importantly, after knockdown of *STK4* gene encoding Mst1 by siRNA, the antifibrotic effect of GI was completely abolished, thus establishing MST1 as its essential functional target. In summary, this study found that GI is a novel MST1 agonist, which alleviates LF by targeting Arg181 residue, restoring Hippo/YAP pathway homeostasis and inhibiting hepatic stellate cell activation, which makes GI a promising candidate drug in the treatment of LF.

1. Introduction

Liver fibrosis (LF) is a key pathological stage in the progression of a variety of chronic liver diseases, such as sclerosing cholangitis, viral hepatitis and nonalcoholic fatty liver disease (NAFLD) [1]. According to statistics, the number of patients with liver fibrosis caused by these diseases in the world has exceeded 1 billion [2]. These liver diseases have a common feature: the liver is in the process of repeated damage and repair for a long time. This continuous cycle of damage and repair will eventually lead to excessive accumulation of extracellular matrix (ECM) and abnormal proliferation of connective tissue in the liver. Over time, these pathological changes will gradually replace the normal liver tissue structure, causing impaired liver function and structural disorder, and eventually developing into LF [3].

Hepatic stellate cells (HSCs) are the main source of myofibroblasts (MFBs) in the liver. Their activation, proliferation and subsequent differentiation into myofibroblasts play a central role in promoting the fibrosis process [4]. After the liver is damaged, HSCs will be activated. This transformation is manifested in the loss of the characteristic star morphology of cells, a decrease in lipid droplets and vitamin A reserves, and a significant increase in the synthesis of extracellular matrix components. These extracellular matrix proteins include type I, type III and type IV collagen, fibrin, layered adhesion protein and a variety of proteoglycans. At the same time, activated hepatic astrocytes will also release a large number of pro-inflammatory factors. This phenotyping is also manifested in the upregulation of α-smooth muscle actin (α-SMA) expression, thus promoting the transition of cells from a resting fat storage-like state to a fibrotic and inflammatory state [5, 6]. Chronic inflammation is a key driver of LF and activation of HSCs. When liver cells are damaged, the surrounding hepatocytes and Kupffer cells will release a series of cytokines and inflammatory mediators. These signals not only directly activate HSCs, but also promote more inflammatory cells to infiltrate the damaged liver tissue. The recruited cells then secrete more inflammatory factors, thus forming a continuous inflammatory microenvironment, further aggravating and strengthening the fibrosis reaction [7]. Therefore, inhibiting the activation of HSCs may be an effective way to delay or even prevent the progression of LF.

The Hippo/YAP signaling pathway is the core pathway for regulating cell proliferation, apoptosis and organ size. It has been confirmed in recent years that it is closely related to the activation of HSCs and the progress of LF [8]. Under physiological conditions, the Hippo pathway kinase cascade (MST1/2-LATS1/2) inhibits its nuclear translocation and the expression of profibrotic target genes (*CTGF*, *ANKRD1*) by phosphorylating the down-

* Corresponding author.
E-mail addresses: xiaoshu2397@163.com (X. Zhang); yuejiayin1990@163.com (J. Yue)
Δ These authors contributed equally to this work.

https://doi.org/10.1016/S1875-5364(26)61217-4
Copyright © 2026, China Pharmaceutical University. Published by Elsevier B.V. All rights are reserved.

stream effector molecule YAP/TAZ [9]. However, in the process of LF, inactivation of Hippo pathway leads to dephosphorylation of YAP and abnormal nuclear entry, which in turn drives HSC activation and excessive deposition of ECM. In addition, recent studies have shown that Yap accumulates significantly in the nucleus at the initial stage of HSC activation; Pharmacological inhibition of YAP has been demonstrated to inhibit HSC activation *in vitro* and slow fibrosis progression *in vivo* [10].

In recent years, natural products have become a hotspot for antifibrotic drug development due to their multi-target regulatory propertie [11]. *Gynostemma pentaphyllum* (Thunb.) Makino is the rhizome or the whole grass of Cucurbitaceae plant gynostemma, which contains saponins, flavonoids, polysaccharides, amino acids, trace elements and other components, and the main active ingredient is gynostemma saponin, whose glycosidic portion is basically dammarane-type tetracyclic triterpenoids [12]. Modern pharmacological studies have demonstrated their broad efficacy, including hepatoprotective and potential antifibrotic activities. However, the specific mechanisms of its monomeric components remain largely unexplored [13, 14]. Our previous structure-activity relationship studies indicated that the aglycone or lower glycosides of gypenosides often exhibit enhanced bioactivity compared to their highly glycosylated precursors. To obtain such core active structures, we optimized an acid hydrolysis process for total gypenosides. This process efficiently yielded a major hydrolysate, gypensapogenin I (GI), which is a characteristic dammarane-type aglycone with a high production yield [15]. Given its structural features and efficient preparation, GI presents itself as an ideal candidate for in-depth pharmacological investigation. Therefore, Our study validated for the first time the antifibrotic effect of GI on human stellate cell line LX-2 and carbon tetrachloride-induced hepatic fibrosis model, and explored the potential mechanism of GI activity. The results showed that GI inhibited HSC activation and ameliorated LF by targeting activation of MST1 to regulate the Hippo/YAP pathway. This study indicates that GI might be a promising therapeutic candidate for the treatment of LF.

2. Materials and methods

2.1. Materials

GI (Fig. 1A) was isolated from *Gynostemma pentaphyllum* (Thunb.) Makino by our laboratory. Saponins from *G. pentaphyllum* (more than 80% content) purchased from Hunan Jiuhui Modern Chinese Medicine Co., Ltd. were hydrolysed using a 3∶2 ratio of aqueous hydrochloric acid. The hydrolysate was purified *via* silica gel column chromatography with a CH_2Cl_2/MeOH gradient (100∶0 to 0∶100, *V*/*V*), followed by further isolation using high-performance liquid chromatography (HPLC). This procedure yielded GI as a white amorphous solid with a purity exceeding 98.5% and a recovery rate of approximately 0.8%, confirming its adequacy for further experimental use. Carbon tetrachloride (CCl_4, ≥ 98.0%, M_r: 153.82; Catalog No.: C805332) was purchased from Macklin Biochemical Company (Shanghai, China). Recombinant human TGF-β1 (Product No.: 100–21) was obtained from PeproTech (Rocky Hill, USA). Silibinin (Sil, ≥ 98% purity, M_r: 482.44; Catalog No.: SJ-MN5167) was sourced from SparkJade Company (Jinan, China).

2.2. Animal model of hepatic fibrosis

Male C57BL/6J mice weighing 20–25g were obtained from Liaoning Changsheng Biotechnology Co. Hepatic fibrosis was induced in six-week-old mice *via* intraperitoneal injection of a 15% CCl_4 solution in olive oil (2 mL·kg^{-1}, three times weekly for 6 weeks; n = 8 mice/group). Mice in the blank control group received an equivalent volume of olive oil only. From the beginning of the fourth week, animals in the treatment groups were administered GI (30 or 60 mL·kg^{-1}) or silibinin (10 mg·kg^{-1}) once daily by oral gavage for a duration of three weeks. Equal amounts of 0.1% CMC-Na solution were given to the blank and CCl_4-treated groups, respectively. At the end of 6 weeks, mice were executed and their livers and sera were collected for subsequent experiments.

All animal procedures conducted in this study were carried out in compliance with the ARRIVE guidelines and received approval from the Animal Use and Care Committee of Shenyang Pharmaceutical University, Shenyang, China (Approval No. SYXK (Liao) 2021-0009).

2.3. Serum ALT/AST

The ALT/AST activity in mouse serum was determined using the assay kits (Product No. S03030, S03040) from Shenzhen Radiometer Life Technology Co.

2.4. Biochemical analysis of liver tissue

Liver tissue samples were homogenized with a tissue grinder. Following homogenization, the samples were centrifuged at 2000 r·min^{-1} for a duration of 20 min, after which the supernatant was collected. Concentrations of interleukin-6 (IL-6), interleukin-1β (IL-1β), and tumour necrosis factor-α (TNF-α) in the liver tissue were quantified using an ELISA assay kit (Wuhan Servicebio Technology Co., Ltd., Wuhan, China).

2.5. Histopathological analysis and immunohistochemistry

Fresh liver tissue samples were isolated and fixed with 4% paraformaldehyde for 24 h. Following fixation, the tissue samples were embedded in paraffin and sectioned at a thickness of 5 μm. These sections were stained using hematoxylin-eosin (HE), Sirius red (SR) and Masson staining kits in order to observe histopathological changes, especially inflammatory infiltration, structural alterations and collagen deposition under a light microscope.

In addition, paraffin embedded sections were subjected to immunohistochemical staining using specific antibodies against type I collagen and α-SMA. Stained sections were observed under a fluorescence microscope (TE 2000, Nikon, Japan) and images were acquired for subsequent evaluation. Quantitative analysis of positive staining areas was done using ImageJ software.

2.6. Hepatic hydroxyproline assay

Hepatic hydroxyproline (HYP) content was measured using a commercially available assay kit (Solarbio, Beijing, China; Cat# BC0250) according to the manufacturer's instructions.

2.7. Cell culture and processing

Human hepatic stellate cells LX-2 cells were purchased from CyberKnife (Shanghai) Biotechnology Co. Cell lines were routinely tested for mycoplasma. LX-2 cells were maintained in DMEM growth medium supplemented with 10% fetal bovine serum (*V*/*V*) and 1% penicillin-streptomycin. These cells were cultured at 37 °C in an air environment with 5% CO_2. For cellular experiments, GI was dissolved in DMSO at a stock concentration of 100 mmol·L^{-1}. LX-2 cells were first pretreated with GI (5, 10, 20, 40, 60, 80, 100 μmol·L^{-1}) for 24 h and then collected. LX-2 cells were first serum-starved for 24 h. Subsequently, the cells were stimulated with 5 ng·mL^{-1} TGF-β1 and either 1–40 μmol·L^{-1} GI or 2.5 μmol·L^{-1} silibinin, and then cultured for another 24 h. The appropriate GI concentration for use in subsequent experiments

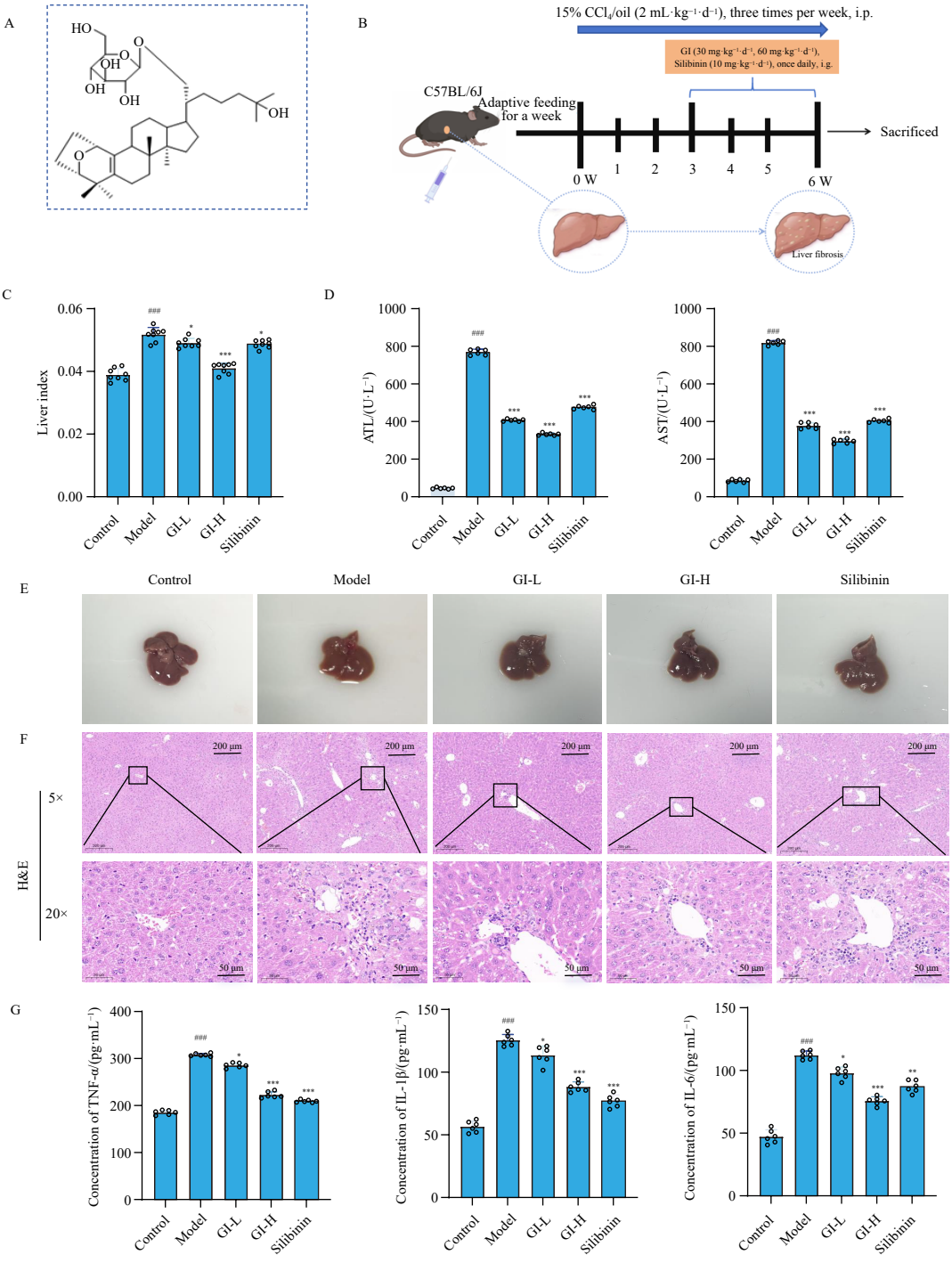


Fig. 1 GI ameliorates CCl_4-induced liver injury. (A) Schematic representation of the chemical structure of GI. (B) Schematic representation of the mouse LF model and treatment with GI or Silibinin. (C) Liver index measurement. Liver weight to body weight ratio was calculated after weighing the mice and their livers (n = 8). (D) Serum ALT and AST levels in mice (n = 6). (E) Gross morphology of liver tissues from each group under identical imaging conditions. (F) Histopathological features of mouse livers detected by HE staining. Magnification: × 5, × 20 (scale bar = 50/200 μm). (G) Levels of TNF-α, IL-1β, and IL-6 inflammatory factors in mouse livers (n = 6). Data are mean ± SD, analyzed by one-way ANOVA with Tukey's test. $^{\#\#\#}P < 0.05$, control *vs* model; $^{*}P < 0.05$, $^{**}P < 0.01$, $^{***}P < 0.001$, treatment *vs* model; ns, not significant.

was determined by CCK-8 assay.

2.8. Wound healing assay

LX-2 cells were seeded in 12-well plates at a density of 2 × 10^5 cells per well. After 24 h, linear scratches were created on the confluent cell monolayer using a 10 μL pipette tip, followed by three washes with PBS. In all groups except the control, TGF-β1 was added to the culture medium together with either GI or Silibinin, and the incubation was continued for 24 h. After that, suck out the culture medium, wash the cells with PBS, and then observe the cell morphology under the inverted microscope and take photos. The image of the scratch healing experiment is analyzed by ImageJ software, the scratch area is measured at different points in time, and then the mobility is calculated according to the following formula:

$$\text{Migration rate}\ (\%) = (A_0 - A_t)/A_0 \times 100\%$$

where A_0 represents the initial wound area at 0 h, and A_t represents the wound area at the indicated time point.

2.9. Immunofluorescence

The tissue sections and LX-2 cells were first deparaffinized

and rehydrated, followed by blocking with 5% goat serum for 30 min at 25 °C. They were then incubated with primary antibodies targeting α-SMA (1∶100) and p-MST1 (1∶100) overnight at 4 °C. After washing with PBS the next day, fluorophore-conjugated secondary antibodies were applied and incubated at 37 °C for 2 h. Following another PBS wash, nuclei were counterstained with 4′,6-diamidino-2-phenylindole (DAPI; 1∶5000, Solarbio, China) for 5 min. Finally, the sections underwent a final PBS wash and were mounted using an anti-fade medium. Imaging was performed with an Olympus inverted fluorescence microscope.

2.10. Western blot assay

Liver tissue (100 mg) stored at −80 °C was homogenized at 4 °C in RIPA lysis buffer containing protease inhibitors and grinding beads, followed by centrifugation at 12 000 r·min^{-1} for 15 min at 4 °C to obtain total protein. Cultured cells were similarly lysed with RIPA buffer, and total protein was collected by centrifugation. Protein concentrations were measured using a BCA assay kit. The samples were separated by 10% SDS-PAGE and transferred onto polyvinylidene fluoride (PVDF) membranes. The membranes were blocked with 5% skim milk and incubated with primary antibodies at 4 °C overnight. After five washes, the membranes were incubated with secondary antibodies at room temperature. Finally, the signals on the membranes were detected using a chemiluminescence imaging analysis system (Beijing Saizhi Chuangye Technology Co., Ltd.) and quantified with ImageJ software.The following antibodies were used: α-SMA and Collagen I (Abcam, Cambridge, UK); Anti-TGF-β (Cohesion Biosciences); Anti-Smad2 (AF6449), Anti-Smad3 (AF6367), Anti-p-Smad2 (AF3447), Anti-p-Smad3 (AF3367), Anti-LATS1 (A11058), Anti-MST1 (DF7691), Anti-YAP (A10012), Anti-p-LATS1 (AF8482), Anti-p-MST1 (AF2367), Anti-p-CTGF (DF7091), Anti-p-ANKRD1 (AF0677) and Anti-p-YAP (AF3325) (Affinity Biosciences, Cincinnati, USA); Anti-β-actin (Wuhan Servicebio Technology Co., Ltd., Wuhan, China).

2.11. Quantitative RT-PCR

Trizol reagent and chloroform were used to extract total RNA from liver tissue. Then, the concentration and purity of RNA were detected by NanoDrop spectrophotometer (Thermo Fisher Scientific, USA). According to the manufacturer's instructions, the mRNA was reverse transcribed into the first strand complementary DNA (cDNA) using a commercial reverse transcription Kit (Servicebio, G3337). The expression levels of *ACTA2*, *COL1A1*, *STK4* (the gene encoding MST1 protein), *LATS1*, *YAP1*, *ANKRD1* and *CTGF* were detected by quantitative real-time PCR, and *GAPDH* was used as internal control. The primer sequences are listed in Supplementary Table 1.

2.12. RNA sequencing and analysis

Total RNA was isolated from liver samples using TRIzol reagent. RNA integrity was assessed using a NanoDrop microspectrometer and agarose gel electrophoresis. Sequencing libraries were constructed from cDNA and sequenced on an Illumina platform by Shanghai Personal Biotechnology Co. Raw sequencing data were subjected to quality control, and low-quality reads were removed. The remaining high-quality reads were aligned to the reference genome using HISAT2 software. Transcript abundance was estimated using HTSeq and normalized as FPKM values. Differentially expressed genes (DEGs) were identified using DESeq2 analysis. To correct for multiple testing, adjusted *P* values (false discovery rate, FDR) were applied. Genes with $|\log_2$ fold change$| > 1$ and $FDR < 0.05$ were defined as significantly differentially expressed. KEGG pathway analysis was used to perform functional enrichment analysis on differentially expressed genes (DEGs). The results were visualized by volcano plots and heatmaps to display the expression patterns of DEGs. This analysis can reveal the intrinsic mechanisms of relevant molecular mechanisms and biological processes under experimental conditions.

2.13. Cell transfection

MST1 is a protein kinase encoded by the *STK4* gene. *STK4* is used to represent gene-level research including mRNA expression analysis and gene silencing experiments. According to the manufacturer's instructions, using siRNA-Mate plus or GP-transfect-Mate transfection reagent (Genepharma, Shanghai, China, Cat. No. G04026/G04008), 75 pM siRNA or 3 μg DNA was transfected into LX-2 cells for 24 h; subsequently, the medium was replaced with medium containing 40 μmol·L^{-1} GI (with or without TGF-β1 at a concentration of 5 ng·mL^{-1}), and the cells were further cultured for 24 h. *STK4*-specific siRNA (forward sequence: 5'-cuuggugcuacacaacagatt-3'; reverse sequence: 5'-ucuguguguagcaccaagtt-3') was synthesized by GenePharma (Shanghai, China).

2.14. Molecular docking

The two-dimensional structure of the small molecule compound GI was drawn using ChemDraw software and subsequently converted into its three-dimensional structure for molecular docking. The 3D structural data of MST1 were obtained from the PDB database (https://www.rcsb.org/) and docked with GI using Autodock software. The docking results were visualized with PyMOL to illustrate the spatial orientation of the ligand within the protein binding pocket. To gain detailed insight into the protein–ligand interactions, the best docking complex was submitted to the online PLIP platform for systematic analysis of key interaction forces [16], including hydrogen bonds, hydrophobic interactions, and halogen bonds.

2.15. Surface plasmon resonance (SPR)

Protein immobilization was performed *via* amine coupling, with MST1 protein fixed on both flow channels of the sensor chip at 10 μL·min^{-1}. Ligand proteins (50 μg·mL^{-1} in pH 4.0 sodium acetate) were used for coupling, after which ethanolamine was injected to block residual sites. GI was then prepared in a series of concentrations in running buffer and injected over the chip from low to high concentration at 30 μL·min^{-1} for 60 s per cycle. The chip was regenerated with 10 mmol·L^{-1} glycine-HCl (pH 2.0) between concentrations. Binding and dissociation constants were derived by globally fitting the data to a 1∶1 Langmuir model using Biacore Insight evaluation software.

2.16. Site-directed mutagenesis and plasmid construction

The full-length human *STK4* (gene encoding MST1) cDNA was cloned into the mammalian expression vector pEX-3 (pGCMV/MCS/Neo). Using this wild-type construct (pEX-3-MST1-WT) as a template, specific arginine-to-alanine substitutions were introduced to generate the mutant constructs: pEX-3-MST1-R148A and pEX-3-MST1-R181A. All constructs, including the empty vector control (pEX-3), were synthesized and sequence-verified by GenePharma Co., Ltd. (Suzhou, China). Wild-type and mutant plasmids were transfected under identical experimental conditions using the same vector backbone and promoter to minimize variability in expression. MST1 protein expression was assessed by Western blot analysis.

2.17. Drug affinity responsive target stability (DARTS) assay

Cell lysates were incubated with GI (20 and 40 μmol·L^{-1}) or

equal volume DMSO at room temperature for 2 h. Then, Streptomyces protease was added in the ratio of 1∶800 and incubated at 37 °C for 30 min. Add an appropriate amount of sample loading buffer and boil in boiling water bath for 10 min to terminate the reaction. Finally, the proteins were isolated by SDS-PAGE and analyzed by Western blotting.

Prior to the formal experiments, the pronase concentration was optimized. Cell lysates were incubated with GI (40 μmol·L^{-1}) or DMSO, followed by digestion with pronase at serial dilutions (1∶200, 1∶400, 1∶00, 1∶1600, and 1∶3200). The residual MST1 levels were detected by Western blot. A 1∶800 dilution of pronase was selected as it yielded the most significant difference between GI and DMSO groups, indicating optimal protection by GI.

2.18. Cellular thermal shift assay (CETSA)

After treating LX-2 cells with GI (40 μmol·L^{-1}) for 24 h, the cells were digested and collected into PCR tubes, approximately 200 μL of medium per group, then placed in a PCR instrument to denature at different temperatures for 5 min, centrifuged, the supernatant was discarded, and washed twice with PBS, then the lysate was added to carry out the routine extraction of proteins, and the binding of drugs to the proteins was observed using Western Blot. Western Blot was used to observe the binding of drugs and proteins.

2.19. Statistical analysis

GraphPad Prism 8.0 software is used for data analysis, and the experimental results are expressed as mean ± standard deviation. Student's t test is used for the difference comparison between the two groups, the one-way analysis of variance (ANOVA) is used for the comparison between multiple groups, and the Dunnett's post hoc test is used for the two-to-two comparison. The significance marks are as follows: $^{*}P < 0.05$, $^{**}P < 0.01$, $^{***}P < 0.001$; $^{\#}P < 0.05$, $^{\#\#}P < 0.01$, $^{\#\#\#}P < 0.001$.

3. Results

3.1. GI ameliorates CCl_4-induced liver injury

In order to study the effect of GI on the development of LF, this study established a mouse model through CCl_4 induction (Fig. 1B). First, C57BL/6J mice were injected with CCl_4 (2 mL·kg^{-1}, 3 times a week, lasting 6 weeks, 8 per group). From the 4th week, the treatment group was given GI (30 or 60 mg·kg^{-1}) or silibinin (10 mg·kg^{-1}) every day for 3 weeks. Serum and liver samples were collected 24 h after the last GI treatment. As shown in Fig. 1C, the liver index of the CCl_4 group was significantly increased compared with the control group, indicating that CCl_4 induced liver hypertrophy. The liver index of the GI group and the Sil group showed a partial recovery, while the liver index of the GI-H group (60 mg·kg^{-1}) almost recovered to a level comparable to that of the control group. Figs. 1D and 1E show that the serum ALT and AST levels were significantly increased in the CCl_4 group, while these markers were significantly reduced in the GI group and the Sil group. Histopathological examination showed obvious structural damage in the livers of CCl_4-treated mice, including a significant increase in degenerated hepatocytes and infiltrating inflammatory cells. However, GI treatment alleviated liver injury in a dose-dependent manner (Figs. 1F and 1G).

To further verify the effect of GI in ameliorating liver injury, we also measured the levels of inflammatory cytokines in mouse serum. The results showed that the protein expression of IL-6, IL-1β and TNF-α was significantly increased in the model group compared with the control group, and significantly down-regulated by the administration of GI (30 and 60 mg·kg^{-1}) and Sil (10 mg·kg^{-1}). Among them, the therapeutic effect of GI (60 mg·kg^{-1}) was superior (Figs. 1H–1J). The above results indicated that GI could inhibit the secretion of inflammatory factors in the livers of mice with CCl_4-induced hepatic fibrosis and attenuate the hepatic inflammatory response.

3.2. GI reduces LF in CCl_4-induced mouse models

In order to evaluate the therapeutic potential of GI for liver fibrosis, Masson's trichrome and Sirius red staining were used to observe collagen deposition. The results showed that compared with the control group, CCl_4 treatment significantly increased collagen deposition, while GI treatment significantly reduced the deposition of fibrosis matrix in the liver of mice (Fig. 2A). The results of immunohistochemistry and Western blot analysis were consistent with the above findings (Figs. 2B–2E). In addition, the liver hydroxyproline content in the model group was significantly increased and significantly decreased after GI treatment (Fig. 2F). These results suggest that GI can effectively improve liver fibrosis *in vivo*.

3.3. GI Inhibits TGF-β1-Induced Activation of Human HSC Line LX-2

The activation and differentiation of HSC is a key link in fibrosis reaction, so we explore whether GI can inhibit HSC activation. TGF-β1 is a classic activator of HSC and a key medium in the progression of LF [17], so we use TGF-β1 to induce LX-2 cell activation, and then give different concentrations of GI for treatment. By detecting cell vitality by CCK-8 method, it was found that GI did not show obvious cytotoxicity in the concentration range of 20–40 μmol·L^{-1}, but cytotoxicity was observed at 50 μmol·L^{-1} (Fig. 3Aa). It is determined that 20 and 40 μmol·L^{-1} are the safe and effective concentration ranges for subsequent *in vitro* experiments. Based on this *in vitro* safety range, the *in vivo* dose of GI is set to 30 and 60 mg·kg^{-1} according to the body surface area. During the three-week administration, there was no significant weight loss, abnormal behavior or death in the mice in the GI treatment group, indicating good safety at these two doses. Then, we evaluated the effect of GI up to 40 μmol·L^{-1} on the proliferation of LX-2 cells induced by TGF-β1. As shown in Fig. 3Ab, TGF-β1 enhances the activation state of LX-2 cells, which is manifested as accelerated cell proliferation; GI treatment can inhibit this effect, and significant inhibition can be observed at 40 μmol·L^{-1}. Accordingly, 20 and 40 μmol·L^{-1} GI are selected for follow-up mechanism experiments.

As shown in Fig. 3B, TGF-β1 stimulation induced obvious cell body enlargement and rapid proliferation of LX-2 cells. On the contrary, GI treatment restored normal cell morphology and significantly reduced the proliferation rate. Since the migration ability reflects the degree of cell activation, we evaluated the effect of GI on the migration of TGF-β1-activated LX-2 cells. The results of wound healing experiment showed that compared with the control group, the number of migrated cells in TGF-β1 group was significantly increased, and high-dose GI significantly reduced the migration ability of TGF- β1 activated cells (Figs. 3C and 3D).

α-SMA is considered a marker of hepatic stellate cell (HSC) activation. We evaluated the expression level of α-SMA in LX-2 cells by immunofluorescence staining. The results showed that TGF- β1 treatment enhanced the expression of α -SMA, but the expression was significantly attenuated after GI administration (Fig. 3E). The same results were obtained in Western blot and qPCR analysis (Figs. 4A–4C).

Smad Protein is a key mediator of TGF-β signaling pathway, which coordinates downstream reactions through receptor-mediated phosphorylation and nuclear translocation. This mechanism

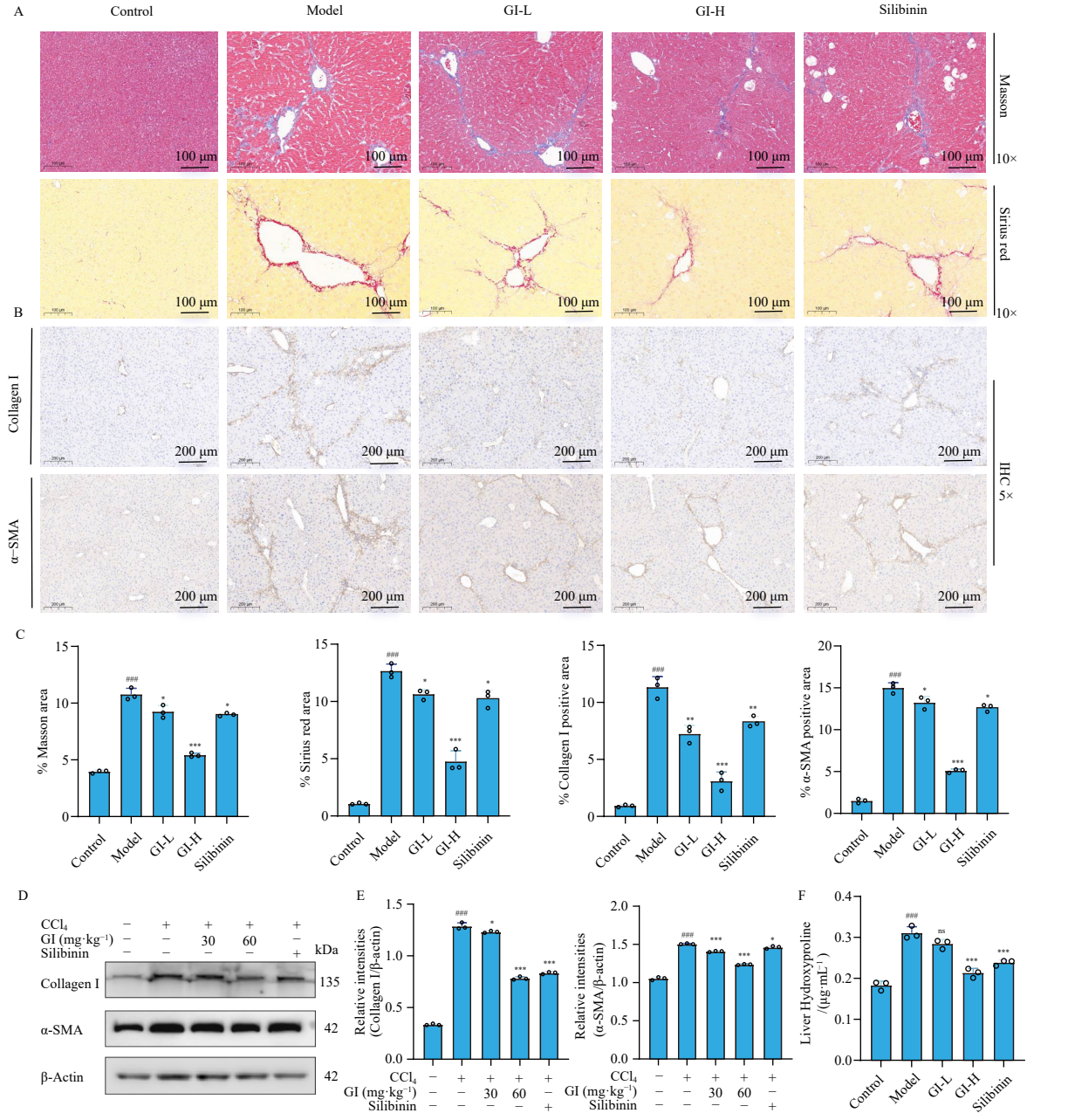


Fig. 2 GI alleviates CCl_4-induced LF in a mouse model. (A) Representative Masson's trichrome and Sirius red staining images of mouse liver tissues in each group. Magnification: × 10; Scale bar: 100 μm. (B) Representative IHC staining of type I collagen and α-SMA in liver tissues of each group. Magnification: × 5; Scale bar: 200 μm. (C) Quantitative analysis of positive staining area using ImageJ software. (D, E) Western blot analysis of type I collagen and α-SMA expression in mouse liver tissues, with β-actin as internal control. (F) HYP content in mouse liver tissues (n = 3). Data are mean ± SD, analyzed by one-way ANOVA with Tukey's test. $^{###}P < 0.05$, control *vs* model; $^{*}P < 0.05$, $^{**}P < 0.01$, $^{***}P < 0.001$, treatment *vs* model; ns, not significant.

can be used as a potential target for anti fibrosis therapy [18]. To explore the molecular mechanism of GI inhibiting HSC activation, we examined its effect on TGF-β/Smad signaling pathway. Western blot analysis showed that TGF-β 1 stimulation significantly increased TGF-β protein expression and Smad2/3 phosphorylation, while GI treatment decreased TGF-β expression and Smad2/3 phosphorylation (Figs. 4D and 4E). In conclusion, GI can inhibit the activation of lx-2 cells induced by TGF-β1.

3.4. Transcriptome analysis of GI key targets

In order to explore the mechanism of GI on LF, RNA sequencing was performed on liver tissues of the experimental group. After the data were normalized by gene expression, the differential genes were detected by deseq tool, and the volcano map was drawn in R language. Compared with the control group, 994 genes were up-regulated and 410 genes were down regulated in the model group; Compared with the model group, 320 were up-regulated and 122 were down regulated in the GI-H group (Fig. 5A). A Venn diagram was constructed based on the analysis of variance results to show the common and unique differentially expressed genes (DEGs) among the groups, and 119 common DEGs were identified between the control and model, and between the model and GI-H (Fig. 5B). Cluster analysis further compared the expression patterns of these 119 overlapping genes in the three groups (Fig. 5C). Among them, literature review showed that among the top 20 key genes, *STK4* (encoding Mst1 protein) was closely related to the activation of hepatic stellate cells and the progression of liver fibrosis [19]. KEGG pathway analysis showed that GI may play a role through Cell entry, Hippo, MAPK signaling pathway, ubiquitin mediated protein degradation and oxidative phosphorylation (Fig. 5D).

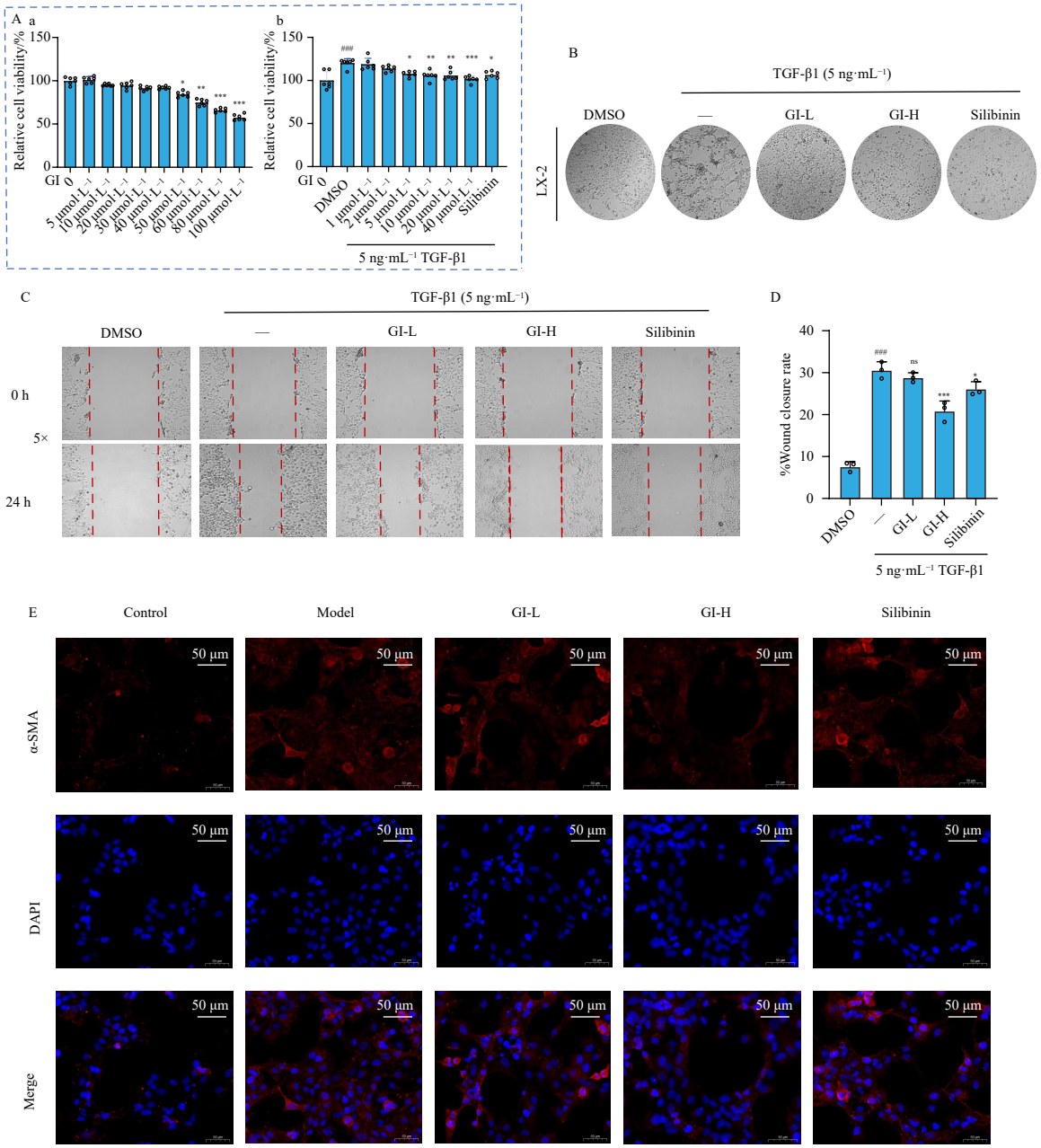


Fig. 3 GI inhibits TGF-β1-induced activation of HSC line LX-2. (A) Representative images of LX-2 cells in each treatment group. (B) CCK-8 method was used to measure the effect of different concentrations of GI on the proliferation of lx-2 cells with or without 5 ng·mL^{-1} TGF-β1 (n = 6). (C, D) microscopic image of LX-2 cell migration evaluated by wound healing experiment (24 h), magnification × 5. (E) Lx-2 cells were immunostained for α-SMA (red) and counterstained for nuclei with DAPI (blue), magnification × 200, scale bar 50 μmol·L^{-1}. Data are mean ± SD, analyzed by one-way ANOVA with Tukey's test. $^{###}P < 0.05$, control *vs* model; $^{*}P < 0.05$, $^{**}P < 0.01$, $^{***}P < 0.001$, treatment *vs* model; ns, not significant.

3.5. GI alleviates LF through the Hippo signaling pathway

Accumulating evidence indicates that the Hippo signaling pathway is critically involved in the progression of liver fibrosis [20,21]. MST1/2, LATS1/2 and YAP are key effector molecules of this signaling pathway [22].To investigate the effect of GI on the Hippo pathway, we first analyzed the expression of MST1, LATS1, and YAP1 in a mouse model of LF. Quantitative PCR analysis revealed that GI treatment significantly increased the expression of *Stk4* and *Lats1*, while decreasing the expression of *Yap1* (Fig. 6A). Western blot results demonstrated that GI administration markedly elevated the levels of phosphorylated LATS1/2 and phosphorylated MST1/2, which act as upstream negative regulators of YAP. Notably, GI treatment also enhanced the phosphorylation of YAP at Serine 397 (Ser-397). Phosphorylation at Ser-397 has been reported to be associated with reduced YAP stability and activity [23] (Figs. 6B and 6C).

Subsequently, we detected the effect of GI on Hippo signaling pathway in LX-2 cells induced by TGF-β1, and the results were consistent with the experiments *in vivo* (Figs. 6D and 6E). In conclusion, GI can activate MSY-LATS-YAP phosphorylation cascade, reduce YAP protein level and inhibit its activity.

3.6. GI and MST1 are stably bound

To further clarify the role of MST1 in GI mediated inhibition of HSC activation, we first used immunofluorescence to detect the expression of phosphorylated MST1 in mouse liver tissue. As shown in Fig. 7A, GI promoted the phosphorylation of MST1. Subsequently, we performed molecular docking analysis to investigate the interaction between GI and MST1, indicating the binding mode of GI to this key target (Fig. 7B). The stable binding config-

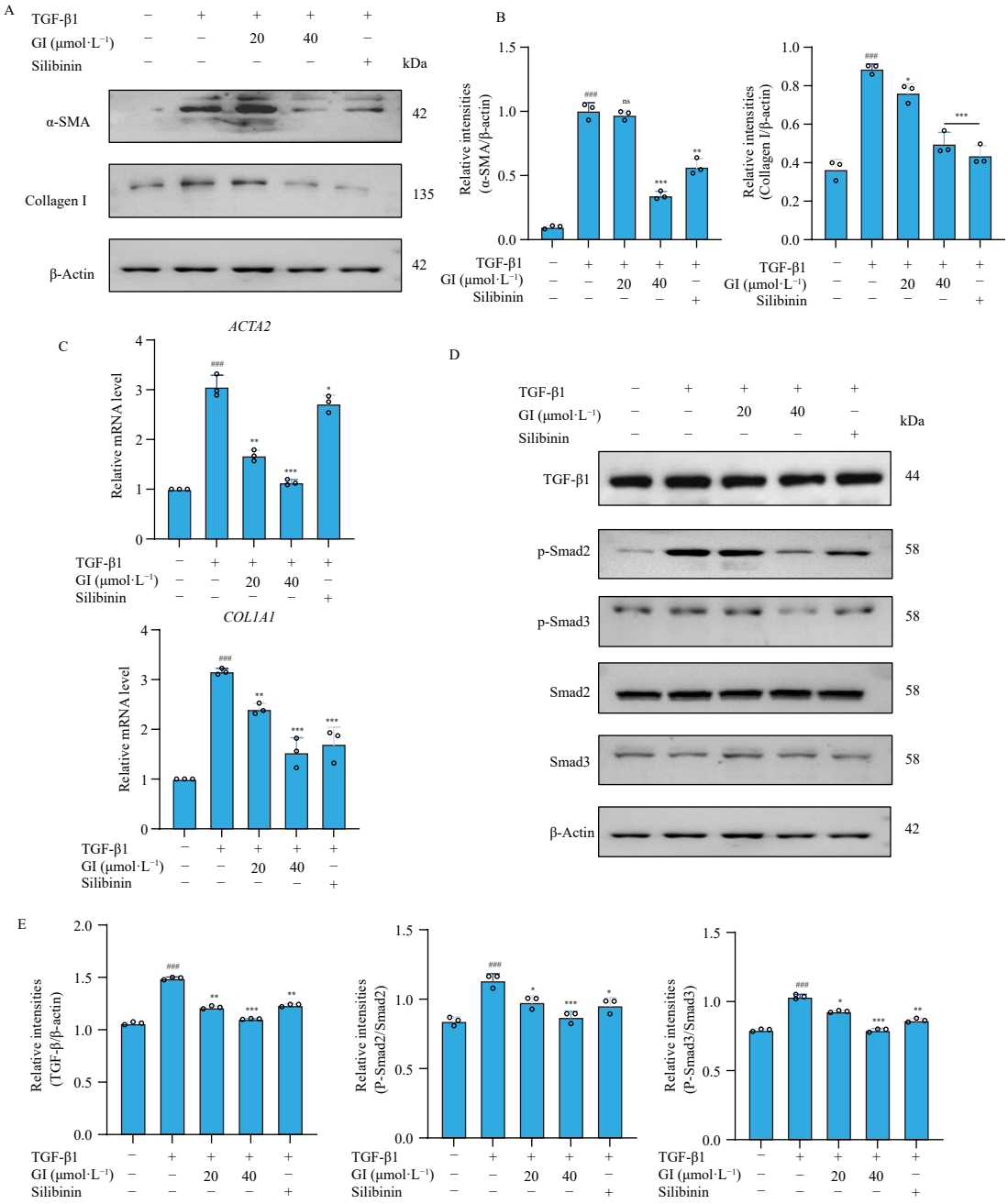


Fig. 4 GI inhibits TGF-β1-induced activation of HSC line LX-2. (A, B) Western blot analysis of Collagen I and α-SMA expression in LX-2 cells. β-Actin was used as an internal control. (C) mRNA expression levels of *ACTA2* and *COL1A1* in LX-2 cells were detected by RT-qPCR. (D, E) The phosphorylation levels of Smad2/3 and TGF-β were analyzed by Western blot (n = 3). Data are mean ± SD, analyzed by one-way ANOVA with Tukey's test. $^{###}P < 0.05$, control *vs* model; $^{*}P < 0.05$, $^{**}P < 0.01$, $^{***}P < 0.001$, treatment *vs* model; ns, not significant.

uration of GI and MST1 was obtained by 3D structure analysis, and the recorded binding energy was −10.4 kcal·mol^{-1}, indicating a strong interaction between the two. PLIP interaction analysis revealed that the small molecule compound GI stably binds to the activation loop of MST1 kinase domain. This binding site overlaps extensively with the key MST1 autophosphorylation sites (Thr276 and Thr282), suggesting that GI may directly regulate MST1 kinase activity by occupying and stabilizing the phosphorylation competent conformation of the activation loop, thereby promoting MST1 phosphorylation. We further verified this combination through SPR, confirming that GI can directly bind to MST1. As shown in Fig. 7C, the equilibrium discomposition constant (K_d) determined by steady-state fitting is 5.29 × 10^{-7} mol·L^{-1}. In addition, we also carried out the drug affinity reaction target stability (DARTS) experiment, which showed that GI treatment enhanced the stability of MST1 and reduced its sensitivity to the digestion of pronase E (Fig. 7D). Subsequently, we further confirmed the interaction between GI and MST1 using cell thermal transformation analysis (CETSA). Under the condition of gradual warming, MST1 in the cells of the GI treatment group showed higher thermal stability. It is worth mentioning that 40 μmol·L^{-1} GI increases the melting temperature (T_m) of MST1 by 3.82 °C, indicating that GI can directly combine with MST1 and enhance its structural stability (Figs. 7E and 7F).

3.7. The Arg181 site of MST1 is critical for GI binding

To verify the precise binding site of GI on Mst1 predicted by molecular docking (the molecular docking analysis is based on the PDB 8A5J structure, in which the key arginine residues are numbered 247 and 280 in the B chain. According to the database correspondence, they correspond to positions 148 and 181 in the

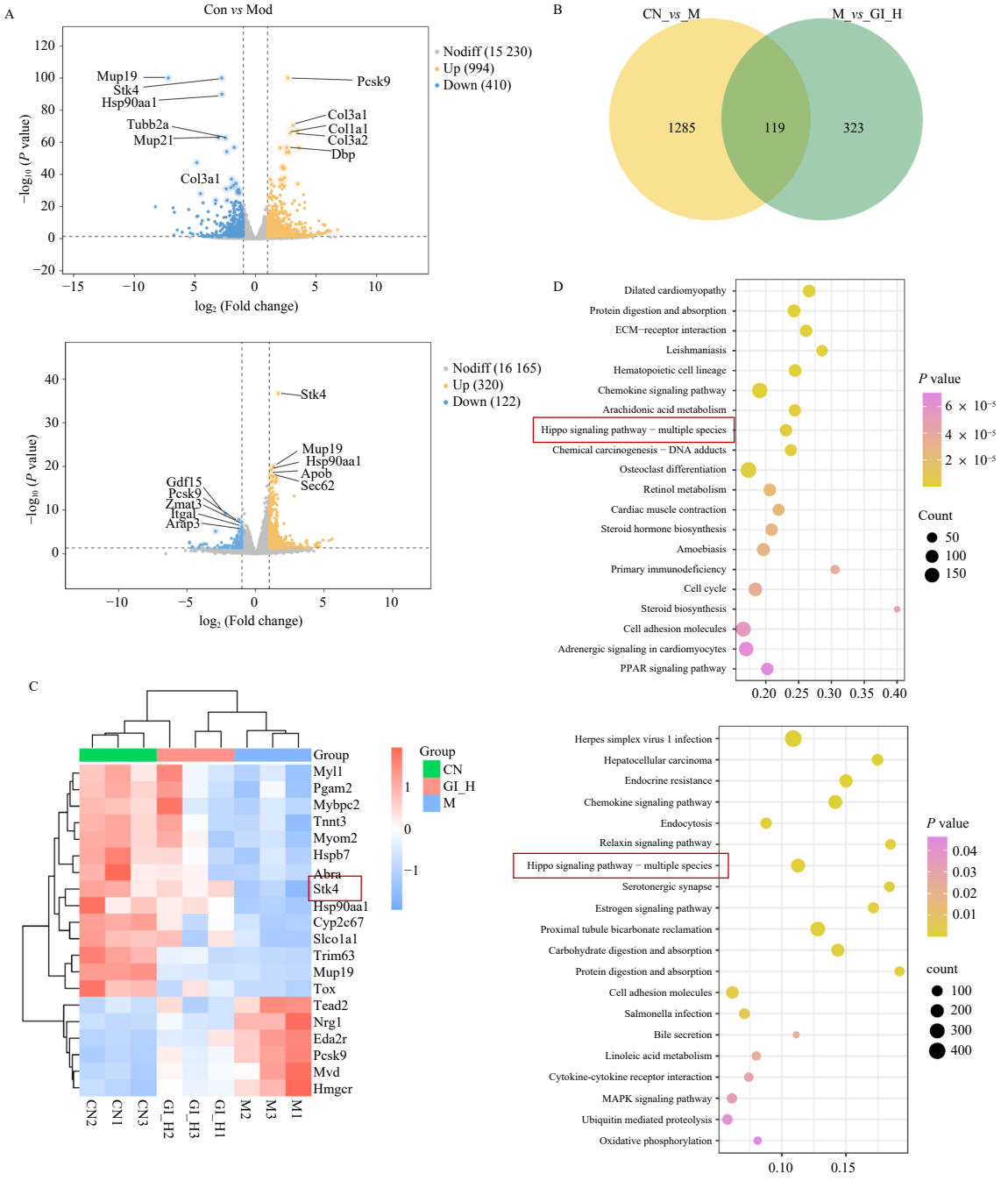


Fig. 5 Transcriptome analysis of GI key targets. (A) Volcano plot of differentially expressed genes (DEGs) between groups. Differentially expressed genes were identified using the threshold of $|\log_2 FC| > 1$ and $P < 0.05$. (B) Venn diagram analysis of DEGs among different groups. Differentially expressed genes were identified using the threshold of $|\log_2 FC| > 1$ and $P < 0.05$. (C) Clustering heatmap of common DEGs between the control and model groups, and between the model and GI-treated groups. (D) KEGG enrichment analysis of comparisons between the model and control groups, and between the model and GI-treated groups.

standard human MST1 protein sequence). We selected these two residues based on the following criteria: (I) they exhibited the lowest predicted binding energy (at −9.8 and −9.2 kcal·mol $^{-1}$) and contributed the most to hydrogen bonding and salt bridge interactions; (II) Arg181 is located near the activation loop, close to the key autophosphorylation site Thr282, while Arg148 is located in the N-terminal regulatory region, which is involved in maintaining the autoinhibited conformation of MST1. The remaining four predicted sites showed high binding energy (> −7.0 kcal·mol $^{-1}$) and were located on the surface far from the functional domain, so they were not preferentially validated. According to this, we constructed two point mutants MST1-R148A and MST1-R181A, targeting arginine residues that form a key salt bridge with phosphorylated threonine. We confirmed that the expression levels of the two mutant proteins in transfected cells were comparable to wild-type (WT) MST1, indicating that these mutations did not affect protein stability (Fig. 8A).

Subsequently, we used the darts experiment to directly evaluate the binding of GI to MST1. In cell lysates expressing wild-type MST1, incubation with GI significantly protected MST1 from pronase digestion, resulting in a stronger residual MST1 signal compared with the control. In sharp contrast, this protective effect completely disappeared in cells expressing the MST1-R181A mutant (Fig. 8B). The MST1-R148A mutant showed a partially reduced but not completely abolished protective effect, suggesting that Arg181 plays a more dominant role in GI binding.

Finally, we investigated the functional consequences of disrupting the GI-MST1 interaction. As expected, GI treatment robustly increased the phosphorylation levels of MST1 , its direct substrate LATS1 and the downstream effector YAP1 in cells ex-

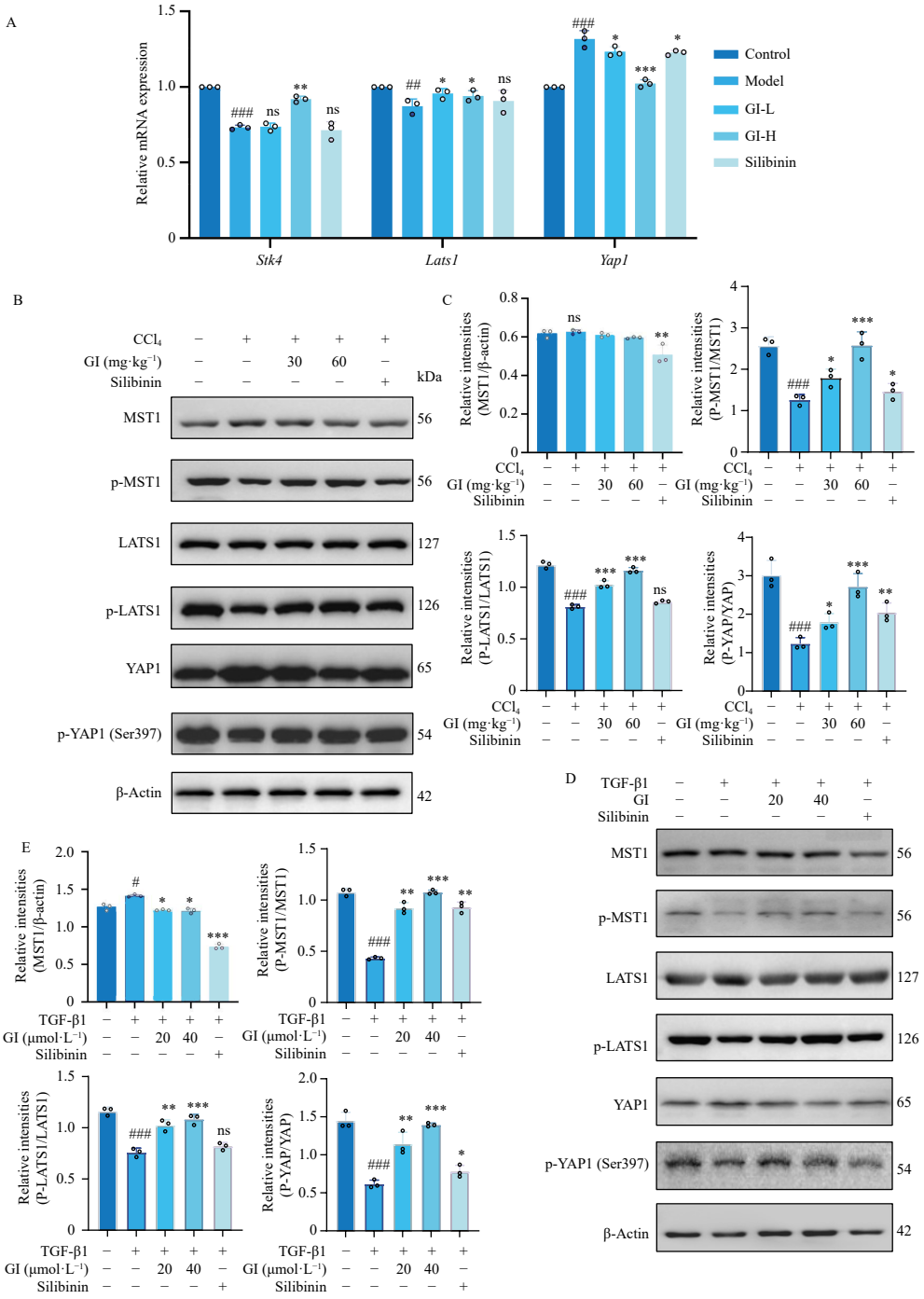


Fig. 6 GI alleviates LF through the Hippo signaling pathway. (A) mRNA expression levels of key genes in Hippo signaling pathway (n = 3). (B, C) protein expression of key components of Hippo signaling pathway in mouse liver. β-actin was used as internal reference (n = 3). (D, E) protein expression of key components of Hippo signaling pathway in LX-2 cells. β-actin was used as internal reference (n = 3). Data are mean ± SD, analyzed by one-way ANOVA with Tukey's test. $^{\#\#\#}P < 0.05$, control *vs* model; $^{*}P < 0.05$, $^{**}P < 0.01$, $^{***}P < 0.001$, treatment *vs* model; ns, not significant.

pressing WT MST1. However, the ability of GI to activate this signaling cascade was severely impaired in cells expressing the MST1-R181A mutant (Figs. 8C and 8D). Consistent with the DARTS results, the R148A mutant exhibited an intermediate phenotype.

In summary, these data suggest that Arg181 residue of MST1 is essential for GI binding and is necessary for GI induced activation of MST1-LATS1-YAP signal axis.

3.8. GI regulates the Hippo signaling pathway by targeting MST1 to alleviate LF

Next, we knocked down *STK4* in LX-2 cells (Figs. 9A and 9B). As expected, when STK4 was knocked down, Gl treatment failed to futher enhance the phosphorylation of downstream targets and inhibit the expression of Collagen I, a-SMA, and other fibrotic markers (Figs. 9C and 9D). Furthermore, numerous studies have demonstrated that *CTGF*, as the most well-established target gene of YAP, is significantly upregulated in fibrotic livers and activated hepatic stellate cells (HSCs). Furthermore, *CTGF* promotes the synthesis and secretion of extracellular matrix (ECM) proteins, particularly fibrillar collagens which constitute the primary components of fibrous deposits [24]. Our data indicated that GI treatment led to a reduction in the expression levels of *CTGF* and *ANKRD1*, which are downstream target genes of YAP, in LX-2 cells. However, upon *STK4* knockdown, GI no longer significantly

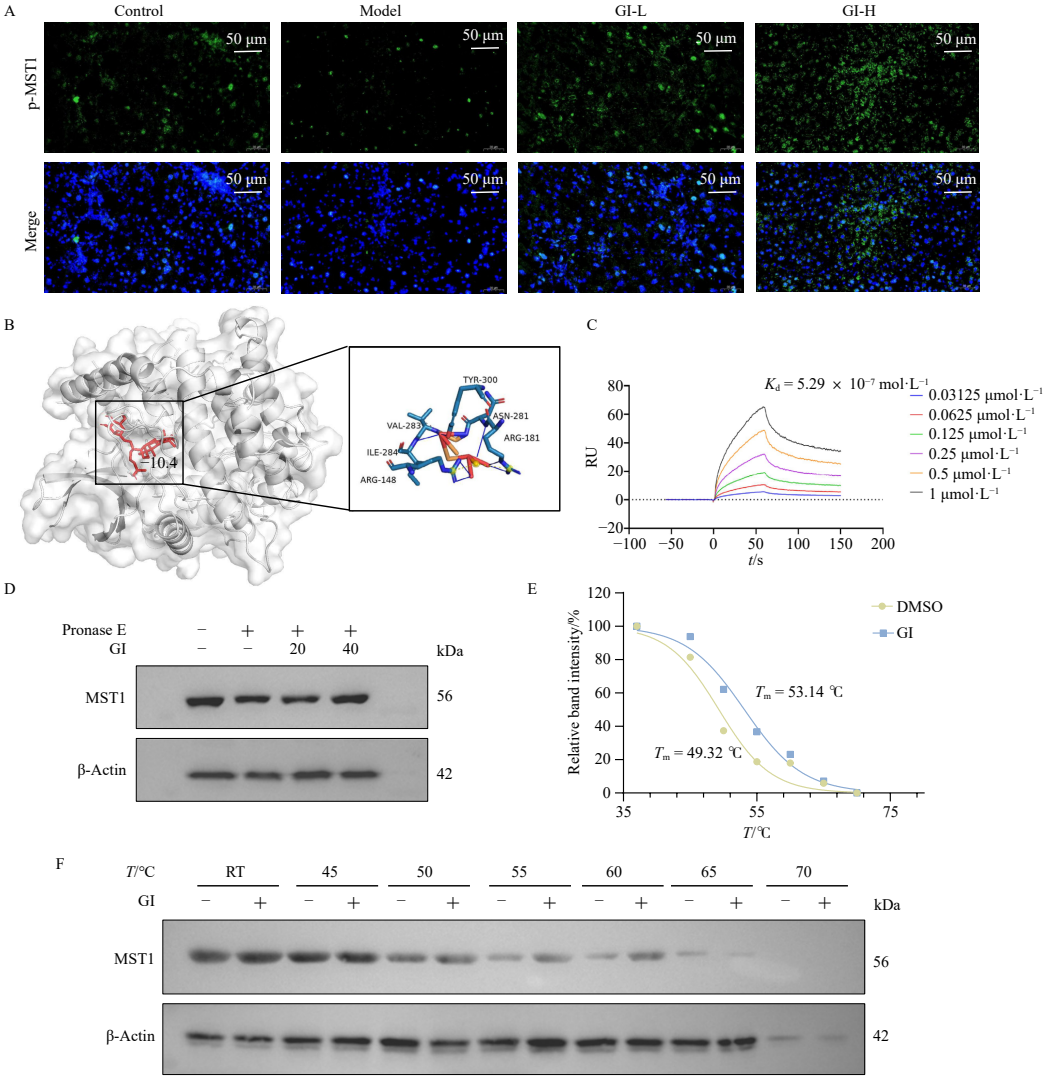


Fig. 7 GI and MST1 are stably bound. (A) Immunofluorescence staining of p-MST1 (green) in mouse liver tissues and counterstaining of nuclei with DAPI (blue). Magnification: × 20; Scale bar: 50 μm. (B) According to the predicted MST1 and GI binding modes by molecular docking, the key residues Arg148 and Arg181 (corresponding to Arg247 and Arg280 of PDB 8A5J B chain, respectively) are highlighted in the figure. (C) SPR technology was used to verify the direct binding characteristics of GI and MST1. (D) The protease sensitivity of MST1 after GI binding was evaluated by DARTS experiments. (E. F) the thermal stability of MST1 after GI binding was analyzed by CETSA.

suppressed the expression of these target genes (Figs. 9E–9G). In conclusion, GI alleviates LF by targeting MST1 and modulating the Hippo signaling pathway.

4. Discussion

This study found that GI is a novel natural compound for anti liver fibrosis. In the body, it can alleviate liver fibrosis; *In vitro*, it can inhibit TGF-β1-induced activation of LX-2 cells. The core mechanism is that GI directly targets MST1 to reactivate the Hippo signaling cascade, thereby inhibiting YAP dependent pro fibrotic signaling. We confirmed that MST1 is a functional molecular target for GI to exert the aforementioned effects through integrated transcriptomic screening, target binding experiments, site directed mutagenesis, kinase activity assays, and functional loss validation.

Hepatic stellate cell activation is a central cellular event in liver fibrosis, characterized by enhanced proliferation, migration, contractility, and extracellular matrix production [25, 26]. In the present study, GI reduced collagen deposition and fibrotic marker expression in CCl_4-induced fibrotic liver tissues and suppressed α-SMA and Collagen I expression in TGF-β1-activated LX-2 cells. These effects were accompanied by attenuation of inflammatory injury and inhibition of TGF-β /Smad signaling pathway, suggesting that GI acts on both pro fibrotic and inflammatory components of liver fibrosis. However, the most important mechanism of this study is that GI does not simply exert general cytoprotective or anti-inflammatory effects; Instead, it acts on a well-defined kinase node MST1, which is upstream of Hippo/YAP signaling and hepatic stellate cell activation.

The Hippo/YAP pathway has become an important signal axis to promote fibrosis in LF [27]. When the Hippo signal is impaired, YAP will accumulate in the nucleus and promote the transcription of fibrosis-promoting genes such as *CTGF* and *ANKRD1*, thereby enhancing HSC activation and extracellular matrix deposition [28, 29]. This study found that GI enhanced the phosphorylation level of MST1, LATS1/2 and YAP, while lowering the expression of YAP downstream target genes. These results show that GI pushes the Hippo/YAP pathway to the YAP inactivation state, thus weakening the transcription procedure required to maintain the continuous activation of HSC. More importantly, knocking down *STK4* largely eliminates the inhibitory effect of GI on the phosphorylation and fibrosis markers of the Hippo pathway, which supports the conclusion that MST1 is necessary for GI to exert anti-fibrosis activity.

Although the expression of *STK4* mRNA was increased in qPCR analysis, the total MST1 protein level did not show a corresponding significant increase by Western blotting. It may be due to post transcriptional regulation, translation regulation, protein stability or other post-translational mechanisms. Importantly,

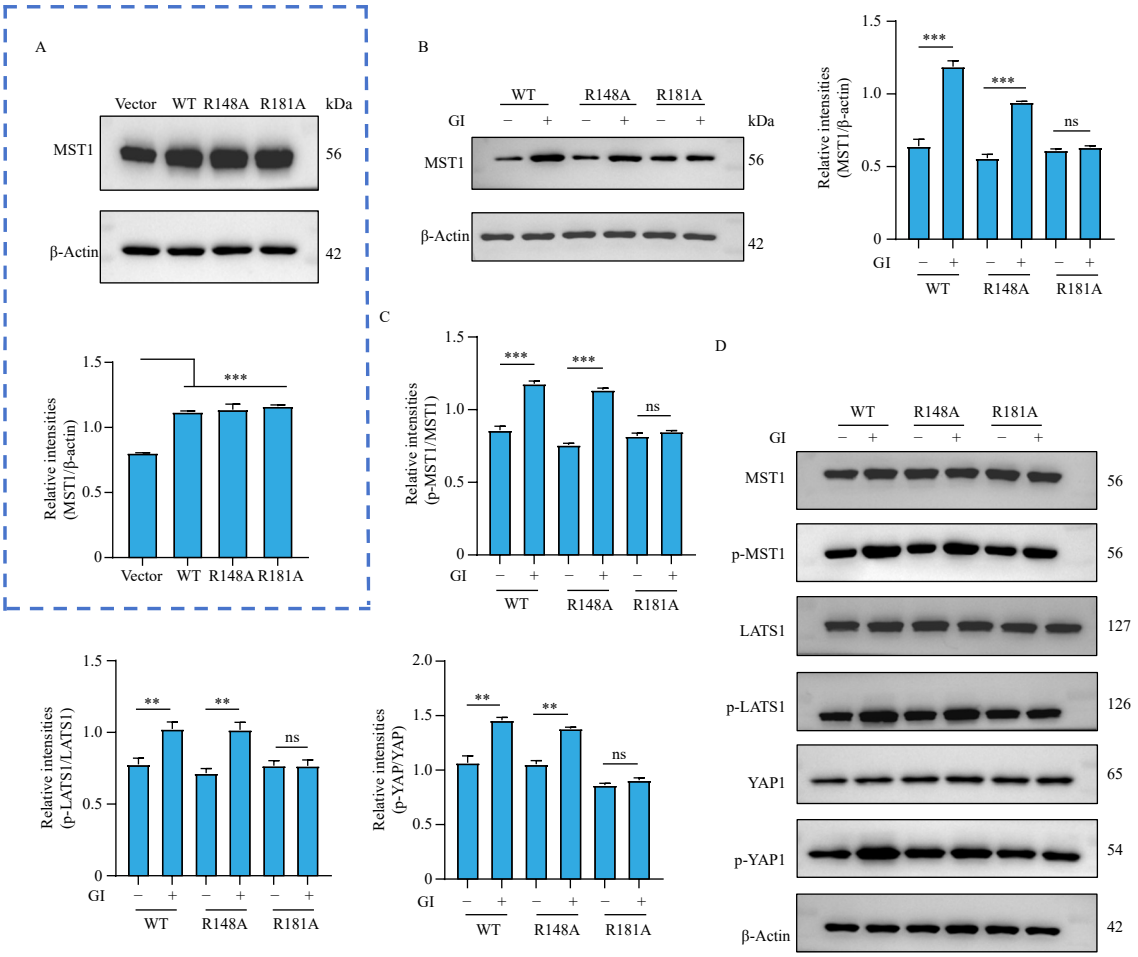


Fig. 8 GI specifically activates MST1 *via* the Arg181 site. (A) Western blot validation of overexpression levels of wild-type and various mutant MST1 proteins in LX-2 cells. (B) Assessment of GI binding affinity to MST1 mutants based on the Drug Affinity Responsive Target Stability (DARTS) assay. (C, D) Western blot analysis of phosphorylation levels of key Hippo pathway molecules in LX-2 cells overexpressing wild-type or R181A mutant MST1 following GI treatment (n = 3). Data are mean ± SD. Data were analyzed using one-way ANOVA followed by Tukey's multiple comparisons test. $^{*}P < 0.05$, $^{**}P < 0.01$, $^{***}P < 0.001$ *vs* control; ns, not significant.

MST1 activity is determined not only by the total protein abundance, but also by its activation state and downstream signaling effect. Therefore, the observed biological effects may be more related to the functional activation of MST1 and the regulation of the Hippo/YAP pathway than just a simple change in the expression level of total MST1 protein.

This study uses a variety of methods to verify that MST1 is the target of GI. Molecular docking predicted a stable interaction between GI and MST1, and SPR confirmed the direct combination of the two. DARTS experiments and CETSA experiments further prove that GI can enhance the protease resistance and thermal stability of MST1 in a cellular environment. These methods reduce the possibility that "MST1 activation is only a downstream result after fibrosis is reduced", indicating that GI directly acts on MST1, thereby activating MST1-LATS1/2-YAP signal cadding. Finally, the mutation experiment identified that Arg181 is a necessary residue for GI to function, so that this target verification is more perfect.

Molecular docking analysis shows that GI binds to the activation ring of the MST1 kinase domain, which is spatially adjacent to the key self-phosphorylation site Thr282. *In vitro* kinase experiments show that GI increases the V_{max} of MST1 by about 1.8 times, while there is no obvious change in K_m, which is the typical feature of heter-configuring activation. Given that the R181A mutation can completely eliminate the effect of GI, we speculate that GI plays a role through a conformational mechanism: stabilizing the active conformation after activated ring phosphorylation, promoting the self-phosphorylation of Thr282, and thus enhancing the catalytic activity. This way of action is similar to that of natural kinase agonists (such as resveratrol and ATM)[30]. Although the transfection efficiency of each mutant has not been directly quantified, the differences between groups have been minimized due to the use of the same plasmid skeleton, promoter and consistent transfection conditions. Both sequencing and Western blot results confirmed the reliability of the integrity of MST1-R148A and MST1-R181A mutants. These controls ensure that the functional differences are mainly due to the point mutation itself, not the difference in transfection efficiency or protein expression levels.

This allosteric mechanism proposed by us has important biological significance: the activation of MST1 provides a direct upstream pathway to inhibit YAP driven Pro fibrotic transcription. GI does not directly inhibit YAP itself, but activates a set of endogenous negative regulatory cascade, which eventually leads to YAP phosphorylation and functional inhibition. Compared with the direct inhibition of YAP transcription, this mechanism may be more advantageous, because the restoration of the upstream kinase cascade can simultaneously affect many downstream processes involved in HSC activation, including proliferation, migration, extracellular matrix formation and inflammation amplification. In addition, these findings also expand the pharmacological value of MST1- although MST1 is often studied as a signal kinase, it is rarely regarded as an anti fibrosis protein that can be directly targeted.

There are still some limitations in this study. In terms of YAP regulation, although GI enhanced YAP phosphorylation and reduced its total protein level, it was not enough to prove that GI promoted YAP degradation. The reduction of YAP may also be

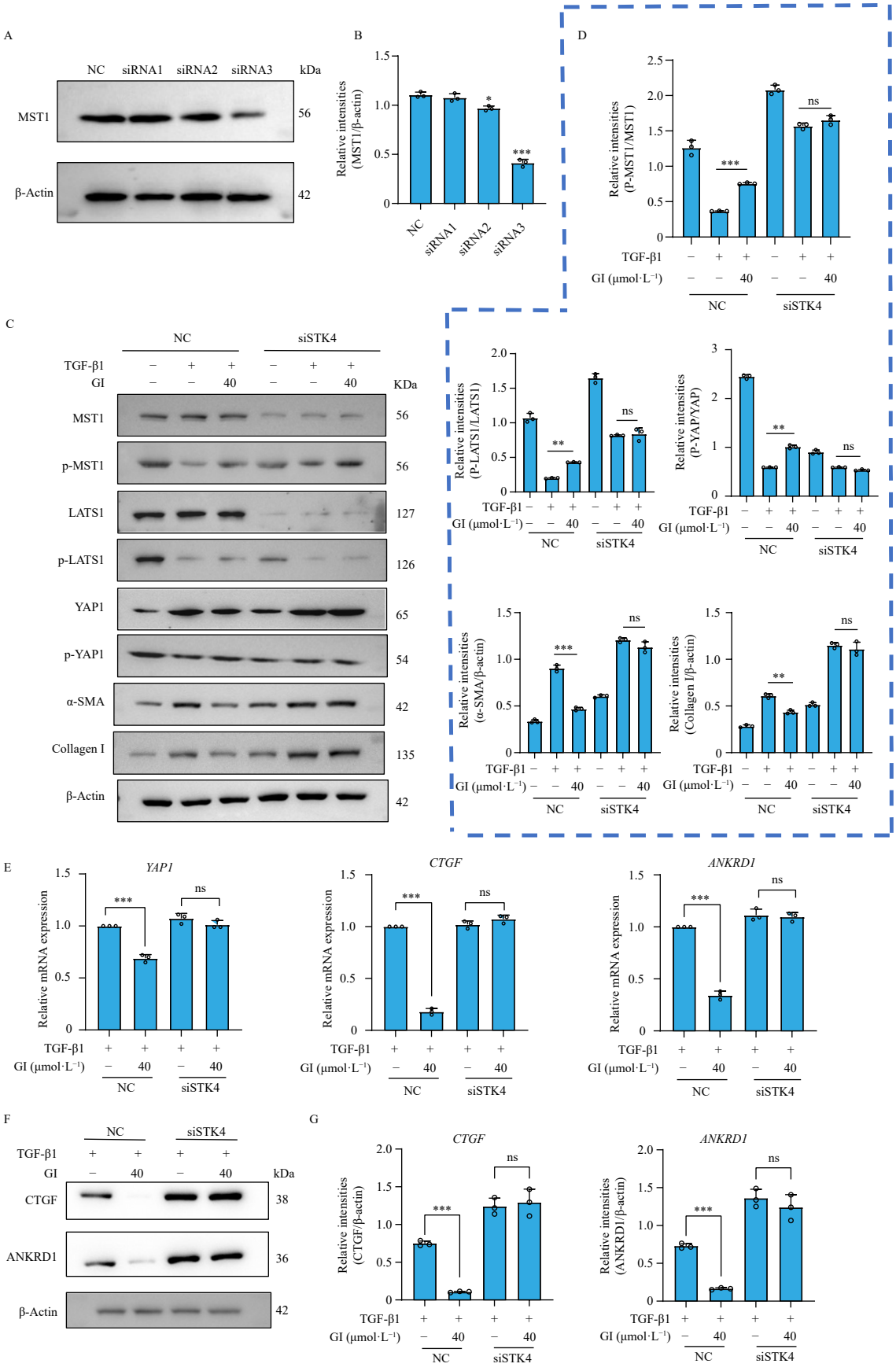


Fig. 9 GI regulates the Hippo signaling pathway by targeting MST1 to alleviate LF. (A. B) Western blot was used to detect MST1 protein expression in LX-2 cells transfected with three kinds of siRNAs (si#1, si#2, si#3). Only si#3 knockout efficiency was high (> 80%), which was used for subsequent experiments. (C, D) The effects of siRNA alone or in combination with GI siRNA on MST1, LATS1, YAP and their phosphorylated proteins, a-SMA and type I collagen, β-actin as an internal reference (n = 3). (E) LX-2 cells were treated with GI (40 μM) without *STK4* siRNA, and the downstream target genes of YAP were detected by RT qPCR. (F, G) The effect of siRNA alone or combined with GI siRNA on *CTGF* and *ANKRD1*, β-actin as the internal reference (n = 3). Data are mean ± SD. Data were analyzed using one-way ANOVA followed by Tukey's multiple comparisons test. $^{*}P < 0.05$, $^{**}P < 0.01$, $^{***}P < 0.001$ *vs* control; ns, not significant.

due to transcription or translation inhibition. In the future, it needs to be clarified by actinomycin tracing, proteasome and lysosome inhibition, ubiquitination analysis and other experiments. In terms of target verification, the conclusion that Arg181 is the direct binding site of GI still depends on indirect evidence such as mutation, darts and enzyme activity detection. R181A mutation may affect protein folding or local conformation rather than specific destruction of binding. The key role of Arg181 can be confirmed by directly comparing purified WT with mutant protein through SPR or ITC, and combining with the complement experiment after knocking down endogenous *STK4*. At the same time, the study lacks the reverse validation of YAP agonists or MST1 inhibitors. In the future, it is necessary to further confirm the causal relationship of MST1-YAP axis by means of pharmacological complementation. At the model level, CCl_4 model can not fully reproduce the etiological diversity of human LF, and the efficacy of GI needs to be verified in metabolic steatohepatitis, cholestatic injury and other models; The discovery of LX-2 cells also needs to be confirmed in primary hepatic stellate cells, liver like organs or patient derived cells. Finally, although GI is well tolerated under the experimental conditions, its pharmacokinetics, metabolism, toxicity and long-term safety still need to be systematically evaluated.

In conclusion, this study shows that GI can reduce LF by directly targeting MST1 and reactivating Hippo/YAP signaling pathway, inhibiting HSC activation and pro fibrosis gene expression. The elucidation of GI-MST1-YAP regulatory axis provides a mechanism basis for the antifibrotic activity of GI, and highlights MST1 as a potential targeted kinase node in LF. These findings not only support the further development of GI or GI derived compounds as candidate antifibrotic drugs, but also suggest that the pharmacological activation of MST1 may represent a promising strategy for restoring Hippo pathway homeostasis in fibrotic liver disease.

Conclusion

In conclusion, this study confirmed that GI can effectively inhibit LF (Supplementary Fig. 10). *In vivo* experiments showed that GI could alleviate liver injury and fibrosis; *In vitro* experiments showed that it could inhibit the activation of hepatic stellate cells. In mechanism, GI directly binds to Arg181 site of MST1 to activate Hippo signaling pathway, and then inhibits the activation of HSCs. Therefore, GI is expected to become a new MST1 agonist and provide a potential choice for the treatment of LF.

Funding

This research was supported by the Liaoning Provincial Department of Education Administration (No.LJ212410163059), Shenyang Pharmaceutical University Spark Project for Cultivating Top Innovative Talents (No.XH2025-07), Liaoning Provincial Science and Technology Program Joint Program (No.2024-MSLH-441), the National Natural Science Foundation of China (No. 32400329), the Natural Science Foundation of Liaoning Province (No. 2024-MS-225), and the Foundation of Liaoning Province Education Administration (No. LJ212410164014).

Supplementary materials

Supplementary data associated with this article can be requested by sending E-mail to the corresponding authors.

Declaration of competing interest

The authors declare that they have no known competing financial interests or personal relationships that could have appeared to influence the work reported in this paper.

References

1 Lambrecht J, Mannaerts I, van Grunsven LA. The role of miRNAs in stress-responsive hepatic stellate cells during liver fibrosis. *Front Physiol*. 2015;6:209. https://doi.org/10.3389/fphys.2015.00209.
2 Asrani SK, Devarbhavi H, Eaton J, et al. Burden of liver diseases in the world. *J Hepatol*. 2019;70:151-171. https://doi.org/10.1016/j.jhep.2018.09.014.
3 Ren S, Chen JM, Wang QL, et al. MicroRNA-744/transforming growth factor β1 relationship regulates liver cirrhosis. *Hepatol Int*. 2019;13:814-825. https://doi.org/10.1007/s12072-019-09993-w.
4 Mederacke I, Hsu CC, Troeger JS, et al. Fate tracing reveals hepatic stellate cells as dominant contributors to liver fibrosis independent of its aetiology. *Nat Commun*. 2013;4:2823. https://doi.org/10.1038/ncomms3823.
5 Lee EJ, Hwang I, Lee JY, et al. Hepatic stellate cell-specific knockout of transcriptional intermediary factor 1 gamma aggravates liver fibrosis. *J Exp Med*. 2020;217. https://doi.org/10.1084/jem.20190402
6 Hazra S, Xiong SG, Wang JH, et al. Peroxisome proliferator-activated receptor γ induces a phenotypic switch from activated to quiescent hepatic stellate cells. *J Biol Chem*. 2004;279:11392-11401. https://doi.org/10.1074/jbc.M310284200.
7 Cubero FJ. Shutting off inflammation: a novel switch on hepatic stellate cells. *Hepatology*. 2016;63:1086-1089. https://doi.org/10.1002/hep.28442.
8 Driskill JH, Pan D. The Hippo pathway in liver homeostasis and pathophysiology. *Annu Rev Pathol*. 2021;16:299-322. https://doi.org/10.1146/annurev-pathol-030420-105050.
9 Yu FX, Guan KL. The Hippo pathway: regulators and regulations. *Genes Dev*. 2013;27:355-371. https://doi.org/10.1101/gad.210773.112.
10 Wang X, Freire Valls A, Schermann G, et al. YAP/TAZ orchestrate VEGF signaling during developmental angiogenesis. *Dev Cell*. 2017;42:462-478.e7. https://doi.org/10.1016/j.devcel.2017.08.002.
11 Parola M, Pinzani M. Liver fibrosis: pathophysiology, pathogenetic targets and clinical issues. *Mol Aspects Med*. 2019;65:37-55. https://doi.org/10.1016/j.mam.2018.09.002.
12 Yuan ZY, Xie MZ, Huang HY. Research progress on plant resources, chemical constituents, and pharmacological effects of *Gynostemma pentaphyllum*. *Asia-Pacific Tradit Med*. 2019;15:190-197. https://doi.org/10.11954/ytctyy.201907063.
13 Bai H, Wang Y, Ge W, et al. Research progress on the anticancer mechanism of isoflavone saponins. *Northwest J Pharm*. 2019;34:564-567. https://doi.org/10.3969/j.issn.1004-2407.2019.04.034.
14 Shen Z, Wang Z, Hou H. New advances in the study of chemical composition, pharmacological effects and application of isoflavones. *Ginseng Res*. 2020;32:59-64. https://doi.org/10.19403/j.cnki.1671-1521.2020.04.014.
15 Li C, Zhang R, Zhan Y, et al. Resveratrol inhibits hepatic stellate cell activation *via* the hippo pathway. *Mediators Inflamm*. 2021;2021:3399357. https://doi.org/10.1155/2021/3399357.
16 Philipp S, Sarah N, Katja L, et al. PLIP 2025: introducing protein-protein interactions to the protein-ligand interaction profiler. *Nucleic Acids Res*. 2025;53:463-465. https://doi.org/10.1093/nar/gkaf361.
17 Tsuchida T, Friedman SL. Mechanisms of hepatic stellate cell activation. *Nat Rev Gastroenterol Hepatol*. 2017;14:397-411. https://doi.org/10.1038/nrgastro.2017.38.
18 Fabregat I, Moreno-Càceres J, Sánchez A, et al. TGF-β signalling and liver disease. *FEBS J*. 2016;283:2219-2232. https://doi.org/10.1111/febs.13665.
19 Fan F, He Z, Kong LL, et al. Pharmacological targeting of kinases MST1 and MST2 augments tissue repair and regeneration. *Sci Transl Med*. 2016;8:352ra108. https://doi.org/10.1126/scitranslmed.aaf2304.
20 Kim CL, Choi SH, Mo JS. Role of the Hippo pathway in fibrosis and cancer. *Cells*. 2019;8:468. https://doi.org/10.3390/cells8050468.
21 Wang X, Zheng Z, Caviglia JM, et al. Hepatocyte TAZ/WWTR1 promotes inflammation and fibrosis in hepatocyte TAZ/WWTR1. *Cell Metab*. 2016;24:848-862. https://doi.org/10.1016/j.cmet.2016.09.016.
22 Dong J, Feldmann G, Huang J, et al. Elucidation of a universal size-control mechanism in Drosophila and mammals. *Cell*. 2007;130:1120-1133. https://doi.org/10.1016/j.cell.2007.07.019.
23 Tu K, Yang W, Li C, et al. Fbxw7 is an independent prognostic marker and induces apoptosis and growth arrest by regulating YAP abundance in hepatocellular carcinoma. *Mol Cancer*. 2014;13:110. https://doi.org/10.1186/1476-4598-13-110.
24 Park S, Kim J, Yang S, et al. Exogenous S1P *via* S1P receptor 2 induces CTGF expression through Src-RhoA-ROCK-YAP pathway in hepatic stellate cells. *Mol Biol Rep*. 2024;51:950. https://doi.org/10.1007/s11033-024-09868-w.
25 Hernandez-Gea V, Friedman SL. Pathogenesis of liver fibrosis. *Annu Rev Pathol*. 2011;6:425-456. https://doi.org/10.1146/annurev-pathol-011110-130246.
26 Li N, Wu CF, Xu XY, et al. Triterpenes possessing an unprecedented skeleton isolated from hydrolyzate of total saponins from *Gynostemma pentaphyllum*. *Eur J Med Chem*. 2012;50:173-178. https://doi.org/10.1016/j.ejmech.2012.01.052.
27 Yasuda D, Kobayashi D, Akahoshi N, et al. Lysophosphatidic acid-induced YAP/TAZ activation promotes developmental angiogenesis by repressing Notch ligand Dll4. *J Clin Invest*. 2019;129:4332-4349. https://doi.org/10.1172/jci121955.
28 Zhang K, Chang Y, Shi Z, et al. Omega-3 PUFAs ameliorate liver fibrosis and inhibit hepatic stellate cells proliferation and activation by promoting YAP/TAZ degradation. *Sci Rep*. 2016;6:30029. https://doi.org/10.1038/srep30029
29 Song H, Li J, Yang H, et al. Enhancement of functional insulin-producing cell differentiation from embryonic stem cells through MST1-silencing. *Diabetol Metab Syndr*. 2025;17:93. https://doi.org/10.1186/s13098-025-01666-z.
30 Lee JH, Guo Z, Myler LR, et al. Direct activation of ATM by resveratrol under oxidizing conditions. *PLoS One*. 2014;9(6):e97969. https://doi.org/10.1371/journal.pone.0097969.